

1                   **Impacts of New Particle Formation on Aerosol Cloud**  
2                   **Condensation Nuclei (CCN) Activity in Shanghai: Case Study**

3  
4   Chunpeng Leng <sup>a</sup>, Qun Zhang <sup>a</sup>, Jun Tao <sup>b</sup>, Hefeng Zhang <sup>c</sup>, Deqin Zhang  
5           <sup>a</sup>, Chen Xu <sup>a</sup>, Xiang Li <sup>a</sup>, Lingdong Kong <sup>a</sup>, Tiantao Cheng <sup>a</sup>, Renjian  
6           Zhang <sup>d</sup>, Xin Yang <sup>a</sup>, Jianmin Chen <sup>a</sup>, Liping Qiao <sup>e</sup>, Shenrong Lou <sup>e</sup>,  
7                                   Hongli Wang <sup>e</sup>, Changhong Chen <sup>e</sup>

8  
9   a. Shanghai Key Laboratory of Atmospheric Particle Pollution and Prevention  
10       (LAP<sup>3</sup>), Fudan-Tyndall Centre, Department of environmental science and  
11       engineering, Fudan University, Shanghai 200433, China;

12   b. South China Institute of Environmental Sciences, Ministry of Environmental  
13       Protection, Guangzhou 510655, China;

14   c. Atmospheric Environment Institute, Chinese Research Academy of Environmental  
15       Sciences, Beijing 100012, China;

16   d. Key Laboratory of Region Climate-Environment Research for Temperate East  
17       Asia, Institute of Atmospheric Physics, Chinese Academy of Sciences, Beijing  
18       100029, China;

19   e. State Environmental Protection Key Laboratory of the Cause and Prevention of  
20       Urban Pollution Complex, Shanghai Academy of Environmental Sciences,  
21       Shanghai 200233, China;

22  
23  
24  
25   \* Corresponding authors: Tiantao Cheng; Jianmin Chen

26   Tel: (86) 21-6564 3230; fax: (86) 21-6564 2080;

27   Email: [ttcheng@fudan.edu.cn](mailto:ttcheng@fudan.edu.cn), [jmchen@fudan.edu.cn](mailto:jmchen@fudan.edu.cn)

## 28 **Abstract**

29 New particle formation (NPF) events and their impacts on cloud  
30 condensation nuclei (CCN) were investigated using continuous  
31 measurements collected in urban Shanghai from 1 to 30 April 2012.  
32 During the campaign, NPF occurred in 8 out of the 30 days and enhanced  
33 CCN number concentration ( $N_{\text{CCN}}$ ) by a factor of 1.2-1.8, depending on  
34 supersaturation (SS). The NPF event on 3 April 2012 was chosen as an  
35 example to investigate the NPF influence on CCN activity. In this NPF  
36 event, secondary aerosols were produced continuously and increased  
37  $\text{PM}_{2.5}$  mass concentration at a rate of  $4.33 \mu\text{g cm}^{-3} \text{ h}^{-1}$ , and the growth rate  
38 (GR) and formation rate (FR) were on average  $5 \text{ nm h}^{-1}$  and  $0.36 \text{ cm}^{-3} \text{ s}^{-1}$ ,  
39 respectively. The newly formed particles grew quickly from nucleation  
40 mode (10-20 nm) into CCN size range.  $N_{\text{CCN}}$  increased rapidly at SS of  
41 0.4-1.0% but weakly at SS of 0.2%. Correspondingly, aerosol CCN  
42 activities (fractions of activated aerosol particles in total aerosols,  
43  $N_{\text{CCN}}/N_{\text{CN}}$ ) were significantly enhanced from 0.24-0.60 to 0.30-0.91 at SS  
44 of 0.2-1.0% due to the NPF. On the basis of the  $\kappa$ -Köhler theory, aerosol  
45 size distributions and chemical composition measured simultaneously  
46 were used to predict  $N_{\text{CCN}}$ . There was a good agreement between the  
47 predicted and measured  $N_{\text{CCN}}$  ( $R^2=0.96$ ,  $N_{\text{predicted}}/N_{\text{measured}}=1.04$ ). This  
48 study reveals that NPF exerts large impacts on aerosol particle abundance  
49 and size spectra, thus significantly promotes  $N_{\text{CCN}}$  and aerosol CCN

50 activity in this urban environment. The GR of NPF is the key factor  
51 controlling the newly formed particles to become CCN at all SS levels,  
52 whereas the FR is an effective factor only under high SS (e.g. 1.0%)  
53 conditions.

54 **Key words:** cloud condensation nuclei, new particle formation, particle  
55 property, urban

56

## 57 **1. Introduction**

58 Atmospheric aerosols exert great impacts on global climate by  
59 affecting the earth's radiation balance through directly scattering and  
60 absorbing solar and terrestrial lights, and indirectly modifying cloud by  
61 acting as cloud condensation nuclei (CCN) (Charlson et al., 1992;  
62 Lohmann et al., 2005). The indirect effect of primary and secondary  
63 aerosols brings up the largest uncertainty to predictions of aerosol  
64 radiative forcing and global climate change (IPCC, 2013). So far, many  
65 studies of field observation and modeling have found that new particle  
66 formation (NPF) significantly impacts aerosols and CCNs at worldwide  
67 locations (Ghan et al., 2001; Spracklen et al., 2006, 2008; Zhang, 2010).

68 Normally, NPF in the atmosphere is identified as the nucleation of gas  
69 phase precursors and subsequent condensational growth, which is a  
70 crucial secondary transformation course (Birmili et al., 2000; Kulmala et  
71 al., 2004). In fact, NPF consists of a complex set of procedures, including

72 the formation of nanometer-size clusters from gaseous vapors, the growth  
73 of these clusters, the removal of growing clusters by coagulation with  
74 pre-existing particles, and the further growth of survived clusters into  
75 aerosol particles, some of which are large enough to become CCN  
76 (McMurry et al., 1983, 2005; Weber et al., 1996). The NPF event can be  
77 effectively characterized by the formation rate (FR) of nucleation mode  
78 particles and the growth rate (GR) of freshly nucleated particles (Kulmala  
79 et al., 2012). On the basis of over 100 field measurements summarized by  
80 Wang et al. (2013), significant gaps still exist regarding both formation  
81 and growth rate outputs. For example, the GR varied in the range of 1-20  
82  $\text{nm h}^{-1}$  and the FR in  $0.01\text{-}10 \text{ cm}^{-3} \text{ s}^{-1}$ . Condensable gaseous precursors  
83 and their coagulation sink responsible for NPF are commonly high in  
84 megacities of developing countries (Mönkkönen et al., 2005; Wu et al.,  
85 2007). Gaseous sulfur is proved to play a vital role in nucleation process  
86 (Petäjä et al., 2009; Kulmala et al., 2013). Atmospheric ammonia can  
87 effectively lower the surface pressure of gaseous sulfuric molecular and  
88 participates homogeneous nucleation with gaseous sulfuric acid and water  
89 vapor (Smith et al., 2004; Sakurai et al., 2005; Gaydos et al., 2005). In  
90 addition, there are other species responsible for NPF such as amines (Yu  
91 et al., 2012; Benson et al., 2011), low-volatile organic vapors (Metzger et  
92 al., 2010; Paasonen et al., 2010; Riipinen et al., 2011; Ehn et al., 2014)  
93 and iodine compounds (O'Dowd et al., 2002; Vuollekoski et al., 2009).

94 The newly formed particles from atmospheric nucleation are often  
95 able to grow into CCN size and further influence cloud properties or even  
96 global climate (Kerminen et al., 2005; Laaksonen et al., 2005;  
97 Wiedensohler et al., 2009). Kerminen et al. (2012) presents a synthesis of  
98 our current (by the end of 2012) knowledge of CCN production  
99 associated with atmospheric nucleation, and concludes that CCN  
100 production associated with atmospheric nucleation is both frequent and  
101 widespread phenomenon in numerous types of continental boundary  
102 layers, and probably also for a large fraction of the free troposphere. The  
103 latest model results show that the NPF events contribute much more to  
104 global aerosol number burden than primary emissions (Merikanto et al.,  
105 2009; Yu et al., 2008). Under numerous atmospheric conditions aerosol  
106 has a positive feedback to CCN number concentration ( $N_{\text{CCN}}$ )  
107 (Ramanathan et al., 2001; Laaksonen et al., 2005), and  $N_{\text{CCN}}$  usually  
108 exhibits a significant increase after NPF (O'Dowd et al., 2001;  
109 Lihavainen et al., 2003; Kuwata et al., 2008; Yue et al., 2011). Due to  
110 various chemical species involved in NPF, the extent of NPF effects on  
111 CCN varied temporarily and spatially (Spracklen et al., 2008; Pierce and  
112 Adams, 2009). The long-term NPF observations were mainly conducted  
113 in Europe and North America, whereas little has been done in developing  
114 countries (Wang et al., 2013). To date, only a few studies have concerned  
115 NPF and its interaction with CCN in China. Yue et al. (2011) reported

116 that the GR of sulfur-poor NPF was on average about 80% larger than  
117 that of sulfur-rich NPF, and the NPF events increased CCN by 0.4-6  
118 times in Beijing, where various source apportionment of  $PM_{2.5}$  was  
119 reported by Zhang et al. (2013). Wiedensohler et al. (2009) found that the  
120 CCN size distribution is dominated by the growing nucleation mode in  
121 Beijing, which accounted up to 80% of the total CCN number  
122 concentration, in contrast to the usually found phenomenon of the  
123 dominance by the accumulation mode.

124 In the present study, we analyze a comprehensive dataset of 1-month  
125 simultaneous measurements of aerosol size spectra,  $N_{CCN}$ , black carbon  
126 (BC), water-soluble ions and gaseous pollutants to understand the NPF  
127 events and their impacts on  $N_{CCN}$  and aerosol CCN activity in an urban  
128 environment of Shanghai, one of the largest cities in China. A closure  
129 study between predicted and measured CCNs is also conducted to  
130 investigate the influence of aerosol chemical composition on its growth to  
131 CCN. An effective CCN prediction model is further developed based on  
132 model-measurement comparison results.

## 133 **2. Experimental**

### 134 **2.1 Observational site**

135 All instruments were mounted on the roof of one building  
136 approximately 20m above the ground in the campus of Fudan University  
137 ( $31^{\circ}18'N$ ,  $121^{\circ}29'E$ ) located in Shanghai. The observational site is

138 mainly surrounded by urban residential areas, where no large local  
139 emission was detected during this study. The East China Sea is  
140 approximate 40 km east of the site. Except CCN, other measurements  
141 conducted synchronously, including aerosol number size distribution  
142 (condensation nuclei (CN) of 10-800 nm), major inorganic water-soluble  
143 ions in aerosol particles, gaseous pollutants and meteorological factors.  
144 Local time (LT) used in this study is eight hours ahead of UTC.

## 145 **2.2 Measurement and instrumentation**

146 A CCN counter (CCN-100, DMT, USA) with continuous flow and  
147 single column (Roberts and Nenes, 2006; Lance et al., 2006) was  
148 employed to monitor CCN concentrations at supersaturated conditions  
149 (SS in the range of 0.07-2%). Before the campaign, the instrument was  
150 calibrated for SS using standard  $(\text{NH}_4)_2\text{SO}_4$  particles. To maintain stable  
151 SS, according to the instrument operation manual, regular calibrations  
152 were also performed for temperature gradient, input and shear airflows  
153 and pressure (Leng et al., 2013). In addition, periodic zero checks were  
154 done to ensure counting accuracy for optical particle counter (OPC)  
155 installed inside the CCN counter. The ambient aerosol was firstly dried by  
156 a dryer (active carbon) to lower relative humidity (RH) below 30%, and  
157 subsequently introduced into the CCN counter (Leng et al., 2013).

158 Aerosol particle size distributions in the size range of 10-800 nm were  
159 measured using a high-resolution scanning mobility particle sizer (SMPS,

160 TSI 3080, USA). Before and after the field campaign, the instrument was  
161 calibrated to maintain accurate particle sizing. The SMPS data are  
162 recorded by AIM (Aerosol Instrument Management) software from TSI  
163 company. The SMPS 3936 (TSI corp.) is employed to track the size  
164 distribution change, in which the CPC 3736 (TSI corp.) is used to count  
165 the number of particle of each size. The neutralizer 3077a (TSI corp.) is  
166 used in the system to provide known charge on the particles going into  
167 the SMPS. The size of the employed impactor is 0.071 cm. Both multiple  
168 charge and the diffusion correction is applied. The inlet information has  
169 been reported in our previously papers (Wang et al., 2009; Huang et al.,  
170 2013).

171 BC was measured by an online monitor of Aethalometer (AE-31,  
172 Magee Scientific Co., Berkeley, California, USA) at a 5-min time  
173 resolution and a 5 l/min airflow rate. According to the strong ability of  
174 BC light absorption at near infrared wavelengths (Hansen et al., 1984;  
175 Weingartner et al., 2003), BC mass is determined using the light  
176 attenuation at 880 nm and the appropriate specific attenuation cross  
177 section proportional to BC (Petzold et al., 1997). The attenuation can be  
178 calculated based on the intensity difference of reference and sensing  
179 beams between light on and off (Dumka et al., 2010). In order to screen  
180 the impacts of other absorptive material, the data contaminated by  
181 mineral and dust aerosols were excluded from BC measurements. Details



182 for instrument operating and calibrating can be found in Cheng et al.  
183 (2010).

184 A monitor of aerosols and gases (MARGA, ADI 2080, Netherlands)  
185 was employed to measure the mass concentrations of major inorganic  
186 water-soluble ions ( $\text{Na}^+$ ,  $\text{K}^+$ ,  $\text{Mg}^+$ ,  $\text{Ca}^+$ ,  $\text{SO}_4^{2-}$ ,  $\text{Cl}^-$ ,  $\text{NO}_3^-$  and  $\text{NH}_4^+$ ) in  
187 ambient aerosol particles at a 1h time resolution. The methods of  
188 sampling, operation and internal calibration of the MARGA were  
189 described in Du et al. (2011).

190 A continuous ambient particulate monitor (FH62C14, Thermo) was  
191 used to measure  $\text{PM}_{2.5}$  (particles in aerodynamic diameter less than 2.5  
192  $\mu\text{m}$ ) concentration online. The Thermo FH62C14 Continuous Ambient  
193 Particulate Monitor (FH62C14) is a radiometric particulate mass monitor  
194 capable of providing real-time measurements. It incorporates  
195 time-averaged measurements of an integral beta attenuation sensor and  
196 advanced firmware to optimize the continuous mass measurement. The  
197 FH62C14 equips a dynamic heating system (DHS) to maintain the  
198 relative humidity (RH) of the air passing through the filter tape of the  
199 radiometric stage well below the point at which the collected particles  
200 accrete and retain liquid water. The DHS system minimizes the internal  
201 temperature rise ensuring negligible loss of semi-volatiles from the  
202 collected sample when the ambient RH is below the threshold to which  
203 the heater is controlling. As the ambient RH increases above the threshold,

204 the applied heating is optimized to maintain the RH threshold above the  
205 beta attenuation filter tape. Necessary sensor calibrations are performed  
206 for temperature, relative humidity, barometric pressure and volumetric  
207 flow regularly to maintain valid measurements.

208 Moreover, an automatic weather station client (HydroMet<sup>TM</sup>, Vaisala)  
209 and a visibility monitor (Belford, M6000) were employed to collect the  
210 data of meteorological variables and atmospheric visibility.

### 211 **3. Results and discussion**

#### 212 **3.1 Overview of the entire period**

213 The ground-based measurements contained  $N_{CCN}$  at SS of 0.2-1.0%,  
214 aerosol size spectra, atmospheric visibility,  $PM_{2.5}$ , BC, aerosol inorganic  
215 water-soluble ions and  $SO_2$  and were conducted during the period of 1-30  
216 April 2012. Figure 1 describes the general meteorological conditions (e.g.  
217 wind speed, wind direction, RH and temperature) for the entire period.  
218 Wind frequently changed direction and were mostly weaker than  $6 \text{ m s}^{-1}$ .  
219 There was no significant precipitation in this month and RH seldom  
220 exceeded 90%. Temperature generally varied between 10-25 °C.

221 Figure 2 shows the temporal variations of 5-min mean  $SO_2$ ,  $PM_{2.5}$   
222 concentration and atmospheric visibility for the entire period. In general,  
223  $PM_{2.5}$  and visibility were negatively correlated and averaged  $70 \pm 60 \mu\text{g}$   
224  $\text{m}^{-3}$  and  $24.3 \pm 23.7 \text{ km}$ , respectively. The maximum and average of  $PM_{2.5}$   
225 in the current study is of less magnitude than those measured in a

226 previous study in 2006 in this urban environment which showed a range  
227 of 17.8-217.9  $\mu\text{g m}^{-3}$  and an average of 94.6  $\mu\text{g m}^{-3}$  (Wang et al., 2006).  
228  $\text{PM}_{2.5}$  frequently experienced a clear inter-day oscillating with a similar  
229 intra-day cycle.  $\text{PM}_{2.5}$  can reflect the variations of ambient particulate  
230 pollutant loadings in the boundary atmosphere layer, and can be viewed  
231 as an additional proxy of pre-existing particle amounts for identifying  
232 NPF. In a broad view, atmospheric visibility frequently declined to be less  
233 than 10 km, revealing heavily polluted episode occurrences (e.g. haze). In  
234 fact, the haze or hazy days accounted for 50% of the study period, during  
235 which atmospheric visibility was on average 5.65 km, while it was 24.3  
236 km on average for the rest of the days.

### 237 **3.1.1 New particle formation event**

238 It has been widely accepted that the key criterion for discerning an  
239 NPF event is to identify an acute burst of nucleation mode particles,  
240 known as newly formed particles up to detectable size of 3 nm exceeding  
241 the background level and lasting for several hours and subsequent growth  
242 in mean particle size (Birmili and Wiedensohler, 2000; Kulmala et al.,  
243 2004, 2012; Vakkari et al., 2011). The supplementary criteria are also  
244 needed for identifying NPF, such as low pre-existing particle loading, an  
245 apparent “banana” shaped particle number concentration as a function of  
246 time and size, and favorable weather conditions essential for excluding  
247 pre-existing particle disturbance particularly in urban environment (Shi et

248 al., 2001; Heintzenberg et al., 2007; Olofson et al., 2009). In this study,  
249 although the SMPS is only capable of capturing particles no less than 10  
250 nm, the aerosol size spectra from the SMPS measurements was available  
251 to determine NPF and to calculate the FR and GR of NPF.

252 In this study, the days with distinct bursts of nucleation mode (10-20  
253 nm) particles lasting for at least 1.5 h from their initial outbreak to  
254 maximum in number concentration, and with apparent growth to larger  
255 sizes (e.g. 20-50 nm) for a few hours, were defined as effective NPF days.  
256 The rest of the days were defined as non-NPF days. Figure 3 shows the  
257 1-month series of aerosol size distribution, 4-min mean total ( $N_{total}$ ) and  
258 nucleation mode ( $N_{10-20nm}$ ) aerosol number concentration and 1 h mean  
259 CCN concentration. On a whole, 8 out of the 30 days were characterized  
260 as the NPF days, which represented an occurrence frequency of 27% and  
261 was much higher than the 5.4% measured by Du et al (2012) at the same  
262 site in winter. Many studies have observed greater NPF frequency in  
263 springtime in northern hemisphere. For example, seasonal NPF pattern  
264 with a spring maximum and winter minimum is typical for all Nordic  
265 stations (Dal Maso et al., 2007; Kristensson et al., 2008; Vehkamäki et al.,  
266 2004). In North China Plain, The number of events was highest in the  
267 spring months (Wang et al., 2013). The high frequency during spring in  
268 urban Shanghai is probably due to high frequency of strong wind from  
269 northern China, which helps removing the pre-existing particles in the

270 atmosphere and further favors the occurrence of new particle formation  
271 events (Wu et al., 2008; Wang et al., 2013).

### 272 **3.1.2 Formation and growth rate, and condensation sink**

273 Formation and growth rates are two essential factors characterizing  
274 NPF events (Yue et al., 2011; Kulmala et al., 2012). The FR rate is  
275 theoretically defined as the mean increase rate of nucleation mode  
276 particle in number concentration as a function of time ( $dN_{\text{nucleation}}/dt$ )  
277 during the nucleation stage of a NPF event. In this paper, due to the losses  
278 of newly-formed nucleated particles caused by coagulation, and the  
279 measurement unavailable for 3-10 nm particles, this calculation only  
280 yielded an “apparent particle formation rate (APFR)” (Du et al., 2012). It  
281 should be noted that this APFR would be an underestimate in comparison  
282 with the actual formation rate. On the other hand, the GR rate refers to the  
283 mean size growing rate of nucleated particles in geometric mean diameter  
284 as a function of time during the growth stage of a NPF event, which has  
285 been described in details elsewhere (Kulmala et al., 2001, 2004b; Dal  
286 Masol et al., 2005). The mode diameter, namely a calibrated geometric  
287 mean diameter automatically made by SMPS itself for all aerosol size  
288 bins instead of only for nucleated particles, is used to calculate particle  
289 growth rate in this study. Similarly, this calculation produces an “apparent  
290 particle growth rate (APGR)”. The APGR would be an overestimate in  
291 comparison with the real growth rate due to inclusion of the GR rate

292 caused by coagulation, which is not related to particle mass increases  
293 (Kerminen and Kulmala., 2002).

294 The condensation sink (CS) describes how rapidly vapor molecules can  
295 condense onto the particles and can be used to represent the pre-existing  
296 particle concentrations (Kulmala et al., 2001). Its values can be directly  
297 calculated from the measured aerosol particle size distributions using  
298 equation (1) as following:

$$299 \quad CS = 2\pi D \sum \beta D_p N \quad (1)$$

300 Where  $D$  is the diffusion coefficient of the condensing vapor,  $\beta$  is the  
301 transitional regime correction factor and can be determined using method  
302 from Fuchs and Sutugin (1971),  $D_p$  is the particle diameter and  $N$  is the  
303 particle number concentration of corresponding size. More explanations  
304 and the derivation process for equation (1) can be seen in many studies  
305 (Kulmala et al., 2001, 2005; Dal Maso et al., 2002, 2005; Gong et al.,  
306 2010; Shen et al., 2011; Gao et al., 2012; Wang et al., 2013), therefore it  
307 was only briefly summarized here. It is worth noting that this calculated  
308 CS might be underestimated compared to the real values because its  
309 derivation is based on the dry particle number size distributions incapable  
310 of necessarily representing ambient wet condition well in this study. The  
311 uncertainty coming from the effect of ambient hygroscopic growth of  
312 aerosols on CS ranges from 5% to 50% (Kulmala et al., 2001).

313 The mean formation and growth rates of NPF events were  $0.40 \text{ cm}^{-3} \text{ s}^{-1}$

314 and  $4.91 \text{ nm h}^{-1}$ , respectively, during the whole campaign. The formation  
315 and growth rates showed a strong location dependence, for example,  
316 higher formation and growth rates have been observed in New Delhi  
317 ( $3.3\text{-}13.9 \text{ cm}^{-3} \text{ s}^{-1}$ ,  $11.6\text{-}18.1 \text{ nm h}^{-1}$ ) and Atlanta ( $20\text{-}70 \text{ cm}^{-3} \text{ s}^{-1}$ ), while  
318 comparable values were measured in Beijing ( $6 \text{ cm}^{-3} \text{ s}^{-1}$ ,  $4 \text{ nm h}^{-1}$ ) for  
319 sulfur-rich aerosol type and ( $2 \text{ cm}^{-3} \text{ s}^{-1}$ ,  $6 \text{ nm h}^{-1}$ ) for sulfur-poor aerosol  
320 type and in Shanghai ( $3.3\text{-}5.5 \text{ nm h}^{-1}$ ) (Kulmala et al., 2004; Mönkkönen  
321 et al., 2005; Yue et al., 2011; Du et al., 2012). The mean CS values were  
322  $0.021 \text{ s}^{-1}$  on the NPF event days and  $0.040 \text{ s}^{-1}$  on the non-event days,  
323 lower than those measured in Beijing ( $0.027 \pm 0.021$  and  $0.047 \pm 0.024$   
324  $\text{ s}^{-1}$ ) and New Delhi ( $0.050\text{-}0.070 \text{ s}^{-1}$ ), and higher than those observed in  
325 Shangdianzi (SDZ, a regional station located in the North China Plain,  
326 about 120 km northeast of Beijing,  $0.020 \pm 0.020$  and  $0.026 \pm 0.018 \text{ s}^{-1}$ ),  
327 and European urban environments including Marseille ( $0.003\text{-}0.015 \text{ s}^{-1}$ ),  
328 Athens ( $0.006\text{-}0.013 \text{ s}^{-1}$ ) and Helsinki ( $0.006 \text{ s}^{-1}$ ) (Kulmala et al., 2005;  
329 Hussein et al., 2008; Wang et al., 2013).

### 330 **3.1.3 NPF impacts on aerosol CCN activity**

331 Pierce and Adams (2007) are the first ones that present the full  
332 theoretical framework on the efficiency of CCN production resulting  
333 from nucleation. To explore the NPF potential influence on CCN, we  
334 further examined the impacts of FR and GR rates in NPF events on  $N_{\text{CCN}}$   
335 and aerosol CCN activity. Table 1 summarizes the  $N_{\text{CCN}}$  enhancement

336 ratios for different FR and GR levels during the entire campaign.

337 It has been widely recognized that  $N_{CCN}$  is positively correlated to  $N_{CN}$   
338 under various atmospheric conditions (Ramanathan et al., 2001;  
339 Laaksonen et al., 2005), and enhancements on  $N_{CCN}$  are expected after  
340 NPF events (O'Dowd et al., 2001; Kuang et al., 2009; Yue et al., 2011).  
341 Theoretically, the high FR rate produces more secondary aerosol particles  
342 (i.e.  $N_{CN}$ ), which may subsequently impact  $N_{CCN}$  if new particles grow  
343 into greater sizes (Ghan et al., 2001; Spracklen et al., 2006, 2008; Zhang,  
344 2010). In this paper, however,  $N_{CCN}$  was insensitive to the FR rate of NPF  
345 at SS of 0.2-0.8%, as indicated by the small differences in  $N_{CCN}$   
346 enhancement ratios under various FR and SS values. This finding agrees  
347 with the results of earlier studies that the nucleation of newly formed  
348 particles within the boundary layer poses a minor impact on  $N_{CCN}$ .  
349 Carslaw et al. (2007) found that  $N_{CCN}$  increased only by 12-17% after a  
350 two order of magnitude increase of nucleation rate in central Europe. A  
351 similar result has been reported in Beijing (Yue et al., 2011). The possible  
352 explanation is in two aspects. The first one is due to the two separate and  
353 self-governed processes in particle formation and subsequent growth. A  
354 high formation rate does not necessarily correspond to a high GR rate  
355 since the newly formed particles may not grow into CCN size with  
356 insufficient time period. The second one is due to coagulation process  
357 between particles which leads to reduced  $N_{CN}$  and further lowers  $N_{CCN}$



358 enhancement ratios. In fact, the impact of FR in NPF on  $N_{CCN}$   
359 enhancement increased with SS (Table 1). The lower critical dry diameter  
360 under higher SS for a given aerosol particle was probably the main reason.  
361 For example, according to the  $\kappa$ -Köhler theory (Köhler., 1936; Petters and  
362 Kreidenweis., 2007), pure NaCl particles can act as CCN only at 65 nm  
363 under SS 0.2%, while it can be activated at 22 nm under SS 1.0%.  
364 Presumably, with the presence of an unrealistic high SS where all  
365 nucleation mode particles (10-20 nm) are activated, the formation rate  
366 would be one controlling factor.

367 On the other hand, what controls a newly formed particle to become a  
368 CCN is its survival probability whether it has enough time to grow into  
369 thermodynamic stable size by competing with the capture and removal of  
370 pre-existing particles (Kerminen et al., 2001; Pierce and Adams, 2007;  
371 Zhang et al., 2012). Toward to this end, the aerosol GR rate of NPF  
372 responsible for this survival probability was observed to exert a valid  
373 effect on  $N_{CCN}$  enhancement ratios. As was found in this study, the  $N_{CCN}$   
374 enhancement ratios at larger GR rate were higher than those at lower GR  
375 rate by a factor of 1.06-1.13 depending on SS.

376 Overall, the  $N_{CCN}$  enhancement ratios due to NPF varied as a function  
377 of FR and GR rates and SS. In real atmosphere, SS varies from exceeding  
378 1.0% in clean-air stratus cloud to slightly less than 0.1% in polluted  
379 conditions (Hudson and Noble, 2014). FR may logically play a vital role

380 in CCN production in the clean-air stratus cloud while exert a minor  
381 impact in polluted conditions. GR is invariably the most important factor  
382 in controlling the extent of newly formed particles in becoming CCN  
383 during NPF.

## 384 **3.2 Characteristics of the typical NPF**

### 385 **3.2.1 Enhancement of nanoparticles**

386 The NPF event spanning the period from 10:00 LT on 3 April to 4:00  
387 LT on 4 April is analyzed in detail to shed some light on the relationship  
388 between NPF and CCN. This NPF event was identified to consist a  
389 nucleation stage (10:00-13:00 LT) and a growth (13:00-4:00 LT) stage  
390 (Fig. 4).

391 Before 10:00 LT on 3 April,  $PM_{2.5}$  was below  $20 \mu\text{g m}^{-3}$  due to the  
392 relatively strong wind speed (e.g.  $6 \text{ m s}^{-1}$ ) favoring pollutant dispersion.  
393 BC was less than  $1 \mu\text{g m}^{-3}$  and atmospheric visibility exceeded 30 km  
394 (Fig. 5 and 6). Apparently, the pre-existing particles of nucleation mode  
395 (10-20 nm) were low (Fig. 7). Newly formed particles increased quickly  
396 in just 1.5 hours from the initial outbreak to the maximum concentration  
397 of  $1800 \text{ cm}^{-3}$  (Fig. 7). During the same time period,  $N_{\text{CCN}}$  increased from  
398 15,000 to  $25,000 \text{ cm}^{-3}$ . The newly formed particles grew in size in the  
399 following periods (the growth stage) due to condensation, heterogeneous  
400 reactions of chemical compounds and coagulation between particles  
401 (Wang et al., 2010). The temporal variations of median, geometric mean

402 and mode diameters for the measured aerosol population are given in Fig.  
403 7. In general, these three diameters were strongly correlated with each  
404 other and increased in size ever since the nucleation burst occurred.  
405 During this period, the wind speed was mostly less than  $2 \text{ m s}^{-1}$ , implying  
406 a weak atmospheric dilution of pollutants.  $\text{PM}_{2.5}$  increased after 17:00 LT  
407 on 3 April, showing a significant enhancement from 38 to  $86 \mu\text{g m}^{-3}$ . In  
408 addition, BC correlated well with  $\text{PM}_{2.5}$ , and they both reduce  
409 atmospheric visibility.

### 410 **3.2.2 Insights into chemical species involved**

411 Several factors likely determine if a chemical species is to act as  
412 nucleation precursor, including its abundance, reactivity and volatility  
413 (Zhang et al., 2012). Gaseous  $\text{H}_2\text{SO}_4$  has been proved to be a key  
414 precursor participating in nucleation process due to its low volatility  
415 (Petäjä et al., 2009; Kulmala et al., 2013), and a necessary condition for  
416 new particle formation is for its molecular concentration exceeding  $10^5$   
417  $\text{cm}^{-3}$  in atmosphere (Weber et al., 1999, Nieminen et al., 2009). The  
418 condensation of gaseous  $\text{H}_2\text{SO}_4$  together with subsequent neutralization  
419 with ammonia plays a dominant role in the growth of Aitken mode  
420 particles, whereas it exerts little contribution to the growth of particles in  
421 accumulation mode (Zheng et al., 2011).

422 However, direct measurement of sulfuric acid in ambient air is still  
423 challenging, appropriate proxies are needed. Petäjä et al. (2009)

424 measured the sulfuric acid and OH concentration in a boreal forest site in  
425 Finland and successfully developed three reasonable proxies for sulfuric  
426 acid concentration by using the measured time series as a foundation.  
427 Their proxies refer to source (i.e. gaseous SO<sub>2</sub>, hydroxyl radical, solar  
428 radiation in 280-320 nm range, and global radiation) and sink (i.e.  
429 condensation sink) terms, and the simplest one is the radiation times SO<sub>2</sub>  
430 divided by condensation sink. In this paper, the source and radiation  
431 terms are unavailable, one may plausibly conjecture similar promotion of  
432 H<sub>2</sub>SO<sub>4</sub> on the basis of its gaseous precursor (e.g. SO<sub>2</sub>) evolution (Zhang  
433 et al., 2012).



435 The particle nucleation event showed a burst of 10-20 nm particles when  
436 SO<sub>2</sub> peaked at 10:00 LT on 3 April, with its mass and molar  
437 concentrations exceeding 4.1 μg m<sup>-3</sup> and 3.8 × 10<sup>10</sup> cm<sup>-3</sup>, respectively (Fig.  
438 8). Afterwards, SO<sub>2</sub> underwent a gradual decrease down to 1.5 μg m<sup>-3</sup>,  
439 and SO<sub>4</sub><sup>2-</sup> correspondingly increased from 8 to 10 μg m<sup>-3</sup>. The good  
440 agreement between SO<sub>2</sub> and nucleation mode particles denotes the key  
441 role of gaseous sulfur in controlling particle nucleation (Zhang et al.,  
442 2012; Kulmala et al., 2013).

443 Besides gaseous sulfur, other nucleation precursors have been proposed  
444 to involve in the critical nucleus formation in numerous environment  
445 conditions (Riipinen et al., 2011; Zhang et al., 2012). For example,

446 atmospheric ammonia can significantly lower the surface vapor pressure  
447 of gaseous sulfuric acid molecular and participate homogeneous  
448 nucleation with gaseous sulfur acid and water vapor. According to the  
449 classical ternary homogeneous theory developed recently, the presence of  
450 ammonia in ppt level significantly enhances nucleation rates (Yu et al.,  
451 2006). Many field measurements and laboratory simulations have  
452 corroborated the crucial role of ammonia in the growth of newly formed  
453 particles (Smith et al., 2004; Sakurai et al., 2005; Gaydos et al., 2005).  
454 Though experimental evidence seems very limited, nitrate has been  
455 reported as a crucial contributor to nanoparticle growth, especially for  
456 10-30 nm particles where nitrate is dominant (Hildebrandt et al., 2012).  
457 Riipinen et al. (2011) combined observations from two continental sites  
458 to show that condensation of organic vapors (i.e. non-volatile and  
459 semi-volatile species) is a crucial factor governing the lifetimes and  
460 climatic importance of the smallest atmospheric particles. Ehn et al.  
461 (2014) find that several biogenic VOCs (e.g. monoterpenes) form large  
462 amounts of extremely low-volatility vapours and further demonstrate that  
463 these low-volatility vapours can enhance (or even dominate) the  
464 formation and growth of aerosol particles over forested regions. In this  
465 paper,  $\text{NO}_3^-$  increased by a factor of 1.33 and  $\text{NH}_4^+$  increased by a factor  
466 of 1.45 during the case NPF event, indicating that the particle growth is  
467 partly driven by the condensation of atmospheric precursors (Fig. 8).

### 468 3.2.3 Aerosol CCN activity enhancement

469 Figure 9 shows the temporal evolutions of  $N_{CCN}$  and aerosol CCN  
470 activity at SS of 0.2-1.0% for the entire period. The enhanced  $N_{CN}$  and  
471 reduced aerosol CCN activity, associated with nucleation mode particle  
472 burst, was observed between 10:00 and 13:00 LT on 3 April. In contrast  
473 to  $N_{CN}$  which increased immediately after the burst of nucleation mode  
474 particles, there was a 4 h delay in the increase of  $N_{CCN}$ . As the newly  
475 formed particles grew into larger sizes, both  $N_{CCN}$  and aerosol CCN  
476 activity increased at various stages under different SS. At a SS higher  
477 than 0.4%,  $N_{CCN}$  peaked at 20:00 LT on 3 April.  $N_{CCN}$  greatly promoted  
478 from 8000-12,000  $\text{cm}^{-3}$  to 13,000-20,000  $\text{cm}^{-3}$  under higher SS, however,  
479 only slightly from 6000 to 7000  $\text{cm}^{-3}$  under lower SS (e.g. 0.2%). Larger  
480 critical dry diameter corresponding to lower SS should be the main  
481 reason. For example, the critical dry diameter for pure  $(\text{NH}_4)_2\text{SO}_4$  particle  
482 was 83 nm at SS of 0.2% and was only 29 nm at SS of 1.0%. The newly  
483 formed particles rarely grew larger than 83 nm in size in this NPF event,  
484 hence less  $N_{CCN}$  enhancement was expected at SS of 0.2%. In summary,  
485 the  $N_{CCN}$  enhancement ratios were 1.17-1.88 depending on SS value. In  
486 Beijing, a larger  $N_{CCN}$  enhancement ratio of 1.4-7 was observed under SS  
487 of 0.07-0.86% caused by NPF (Yue et al., 2011).

488 In comparison with  $N_{CCN}$ , aerosol CCN activity was more sensitive to  
489 aerosol size spectra and meteorology factors, which exerts a big

490 complexity into the temporal variation of aerosol activation. Aerosol  
491 activities were effectively reduced by abundant ultra-fine aerosol particles  
492 (CCN-inert) produced during the nucleation period. The minimum  
493 (0.2-0.6) of aerosol activities was found at 13:00 LT on April when the  
494 particle growth started. Owing to the high survival probability of particles  
495 growing from nucleation mode to accumulation mode (CCN size),  
496 aerosol activities began to increase at different steps for varying SS and  
497 reached their maximums of 0.3-0.9 (0.2-1.0% SS) at 4:00 LT on 4 April,  
498 eight hours after  $N_{CCN}$  peaked.

#### 499 **3.2.4 Towards CCN closure for NPF**

500 A kappa value  $\kappa$  describing particle hygroscopicity, firstly  
501 introduced by Petters and Kreidenweis (2007), was employed here to get  
502 CCN closure study during NPF. Assuming aerosol particle population is  
503 totally internal-mixed, the effective integrated  $\kappa$  can be obtained through  
504 weighting their chemical compound volume fractions,

$$505 \quad \kappa = \sum_i \varepsilon_i \kappa_i \quad (2)$$

506 where  $\varepsilon_i$  is the volume fraction of chemical compounds in particles,  
507 and  $\kappa_i$  is the effective  $\kappa$  of individual chemical composition. This  
508 equation has been widely used and described in detail elsewhere (Petters  
509 and Kreidenweis., 2008; Yue et al., 2011). Aerosol particle  
510 compositions were classified into three categories, and  $\kappa_i$  and  $\varepsilon_i$  for  
511 individual composition are listed in Table 2, of which “others” refers to

512  $\text{PM}_{2.5}$ -( $\text{SO}_4^{2-} + \text{NO}_3^- + \text{NH}_4^+ + \text{Cl}^- + \text{Na}^+$ ), and is viewed as a chemical  
 513 compound with  $\kappa_i=0$  (Yue et al., 2011). Due to MARGA data limitations,  
 514 we only attempted to get CCN closure for the case NPF event in this  
 515 study. The hourly mean  $\kappa$  values were varying from 0.19 to 0.42, and had  
 516 an average of 0.28 during the case NPF event. In total, 83.2% of the  
 517 effective  $\kappa$  was explained by  $\text{SO}_4^{2-} + \text{NO}_3^- + \text{NH}_4^+$ , with their individual  
 518 contributions of 37.4%, 27.5% and 18.3%, respectively. By using the  
 519 calculated  $\kappa$ , the critical dry diameter for a particle to act as CCN at a  
 520 given SS can be determined from an extended  $\kappa$ -Köhler theory:

$$521 \quad S(D) = \frac{D^3 - D_d^3}{D^3 - D_d^3(1 - \kappa)} \exp\left(\frac{4\sigma_{s/a}M_\omega}{RT\rho_\omega D}\right) \quad (3)$$

522 where  $\rho_\omega$  is the density of water,  $M_\omega$  is the molecular weight of water,  
 523  $\sigma_{s/a}$  is the surface tension of the solution/air interface,  $R$  is the universal  
 524 gas constant,  $\kappa$  is the hygroscopicity parameter,  $T$  is temperature,  $D$  is the  
 525 diameter of the droplet and  $S(D)$  is the critical dry size under a given SS.  
 526 More explanation and the derivation process of equation (3) have been  
 527 given in detail by Petters and Kreidenweis (2007), therefore there is only  
 528 brief summarization here. The CCN population can be effectively viewed  
 529 as a subset of measured aerosol size distributions since the operating  
 530 range includes the majority of atmospheric particles (10-800 nm).  
 531 Computed for  $\sigma_{s/a}=0.072 \text{ J m}^{-2}$  and  $T=298.15 \text{ K}$ , the predicted CCN  
 532 number concentration can be calculated through integration between the  
 533 bottom and top critical dry diameters (i.e.  $S(D)$ ).



534 Figure 10 provides correlation analysis for the hourly-averaged (N=90)  
535 predicted and measured  $N_{\text{CCN}}$  at SS of 0.2-1.0%. The agreement was  
536 excellent between the predicted and measured  $N_{\text{CCN}}$ , and a linear  
537 regression produced a slope of 0.98 and an intercept of  $-150 \text{ cm}^{-3}$ , with a  
538 correlation coefficient ( $R^2$ ) of 0.96. The ratio of  $N_{\text{predicted}}/N_{\text{measured}}$  varied  
539 between 0.83 and 1.28 with an average of 1.04.

#### 540 **4. Conclusions**

541 The new particle formation (NPF) events and their impacts on the  
542 abundance and properties of cloud condensation nuclei (CCN) were  
543 investigated using 1-month continuous measurements collected in  
544 downtown Shanghai from 1 to 30 April 2012. The NPF events were  
545 observed in 8 out of the 30 days, and their formation and growth rates  
546 were  $0.40 \text{ cm}^{-3} \text{ s}^{-1}$  and  $4.91 \text{ nm h}^{-1}$  on average, respectively. The growth  
547 rate is important in controlling the conversion of newly formed particles  
548 in NPF to possible CCN, whereas the formation rate is viewed as an  
549 effective factor only at higher SS (e.g. 1.0%). This is due to the small  
550 critical dry diameters for particles to act as CCN under high SS  
551 conditions.

552 The NPF event on 3 April 2012 showed that aerosol particle  
553 enhancement in number concentration significantly relates to the length  
554 of nucleation period of NPF, and aerosol particle enhancement in mass  
555 concentration depends on the growth period. The nucleation period leads

556 to increased  $N_{\text{CN}}$  and reduced aerosol activity, while the increases in  $N_{\text{CCN}}$   
557 and aerosol activity occurred during the growth period. The newly  
558 formed particles needed enough time to grow into CCN size and thus  
559  $N_{\text{CCN}}$  had a delayed peak compared to  $N_{\text{CN}}$ .

560 Closure between the measured and predicted  $N_{\text{CCN}}$  is successful  
561 during the NPF event ( $R^2=0.96$ ).  $\text{SO}_4^{2-}+\text{NO}_3^-+\text{NH}_4^+$  explained the  
562 majority of the effective  $\kappa$ , and minimized the impact of lacking  
563 organic matter. An overestimation of 4% for  $N_{\text{CCN}}$  is probably  
564 introduced by the following uncertainties: (1) aerosol assumed to be  
565 completely internal-mixed, which is an unrealistic condition and hardly  
566 realized in real atmosphere, (2) errors introduced by  $\kappa_i$  for individual  
567 chemical composition, and (3) the category “others” typically includes  
568 organic carbon (OC), elemental carbon (EC), hydrophobic inorganic and  
569 other species. Among these other species there are water soluble species  
570 contributing to CCN formation. For example, OC has an effective  $\kappa$  value  
571 of roughly 0.1 and has been reported to be an important contributor to  
572 particle condensational growth. The reasonable closure identified in this  
573 study implies that the detailed information of particle size spectra can  
574 build an effective CCN prediction model, and size plays a dominant role  
575 in aerosol activity during NPF.

576 It should be noted that the contribution of NPF to CCN has not been  
577 fully characterized in this study. For example, the loss of nucleation mode

578 particles by coagulation and the impact of atmospheric dilution and  
579 boundary layer evolution on pre-existing and newly formed CCN are  
580 unknown. To fully determine NPF contribution to CCN, additional  
581 information on size-resolved aerosol composition, size spectra for 3 nm  
582 or smaller particles, atmospheric sink and physicochemical process will  
583 be needed.

584

## 585 **Acknowledgements**

586 This research is supported by the project of “China Fog-haze monitoring  
587 and its numeric forecast operational system at various scales”  
588 (2014BAC16B01) , the National Natural Science Foundation of China  
589 (41475109, 21190053, 21177025, 21277028, 21377029), and partly by  
590 the Research and Development Special Fund for Public Welfare Industry  
591 (Meteorology) of CMA (GYHY201006047), the Shanghai Science and  
592 Technology Commission of Shanghai Municipality (12DJ1400100,  
593 12DZ2260200), the Jiangsu Collaborative Innovation Center for Climate  
594 Change, and Priority fields for Ph.D. Programs Foundation of Ministry of  
595 Education of China (0110071130003), and the national non-profit  
596 scientific research program for environmental protection (201409008).

597

## 598 **Reference**

599 Asmi, A., Wiedensohler, A., Laj, P., Fjaeraa, A. M., Sellegri, K., Birmili,

600 W., Weingartner, E., Baltensperger, U., Zdimal, V., Zikova, N., Putaud,  
601 J.-P., Marinoni, A., Tunved, P., Hansson, H.-C., Fiebig, M., Kivekäs, N.,  
602 Lihavainen, H., Asmi, E., Ulevivius, V., Aalto, P. P., Swietlicki, E.,  
603 Kristensson, A., Mihalopoulos, N., Kalivitis, N., Kalapov, I., Kiss, G., de  
604 Leeuw, G., Henzing, B., Harrison, R. M., Beddows, D., O'Dowd, C.,  
605 Jennings, S. G., Flentje, H., Weinhold, K., Meinhardt, F., Ries, L., and  
606 Kulmala, M.: Number size distributions and seasonality of submicro  
607 particles in Europe 2008-2009, *Atmos. Chem. Phys.*, 11, 5505-5538,  
608 doi:10.5194/acp-11-5505-2011, 2011.

609 Benson, D. R., Yu, J. H., Markovich, A., and Lee, S. -H.: Ternary  
610 homogeneous nucleation of H<sub>2</sub>SO<sub>4</sub>, NH<sub>3</sub>, and H<sub>2</sub>O under conditions  
611 relevant to the lower troposphere, *Atmos. Chem. Phys.*, 11, 4755-4766,  
612 doi:10.5194/acp-11-4755-2011, 2011.

613 Birmili, W., and Wiedensohler, A.: New particle formation in the  
614 continental boundary layer: meteorological and gas phase parameter  
615 influence, *Geophys. Res. Lett.*, 27, 3325-3328, doi:  
616 10.1029/1999GL011221, 2000.

617 Carslaw, K. S., Spracklen, D. S., Kulmala, M., Kerminen, V. -M., Sihto,  
618 S. L., and Riipinen, I.: The impact of boundary layer nucleation on  
619 global CCN, *Aip. Conf. Proc.*, 911-915, 2007.

620 Cheng, T. T., Han, Z. W., Zhang, R. J., Du, H. H., Jia, X., Wang, J. J., and  
621 Yao, J. Y.: Black carbon in a continental semi-arid area of Northeast

622 China and its possible sources of fire emission, *J. Geophys. Res.*, 115,  
623 D23204, doi: 10.1029/2009JD013523, 2010.

624 Cheng, Y., Lee, S. C., Ho, K. F., Wang, Y. Q., Cao, J. J., Chow, J. C., and  
625 Watson, J. G.: Black carbon measurement in a coastal area of south  
626 China, *J. Geophys. Res.*, 111, D12310, doi: 10.1029/2005JD006663,  
627 2006.

628 Dal Maso, M., Kulmala, M., Lehtinen, K. E. J., and Mäkelä, J. M.:  
629 Condensation and coagulation sinks and formation of nucleation mode  
630 particles in coastal and boreal forest boundary layers, *J. Geophys. Res.*,  
631 107, doi:10.1029/2001JD001053, 2002.

632 Dal Maso, M., Kulmala, M., Riipinen, I., Wagner, R., Hussein, T., Aalto,  
633 P. P., and Lehtinen, K. E. J.: Formation and growth of fresh atmospheric  
634 aerosols: eight years of aerosol size distribution data from SMEAR II,  
635 Hyttiala, Finland, *Boreal Env. Res.*, 10, 323-336, 2005.

636 Dal Maso, M., Sogacheva, L., Aalto, P. P., Riipinen, I., Komppula, M.,  
637 Tunved, P., Korhonen, L., Suur-Uski, V., Hirsikko, A., Kurtén, T.,  
638 Kerminen, V. -M., Lihavainen, H., Viisanen, Y., Hansson, H. -C., and  
639 Kulmala, M.: Aerosol size distribution measurements at four Nordic  
640 field stations: identification, analysis and trajectory analysis of new  
641 particle formation bursts, *Tellus*, 59B, 350-361, 2007.

642 Draxler, R. R., and Rolph, G. D.: HYSPLIT (Hybrid Single-Particle  
643 Lagrangian Integrated Trajectory) Model access via NOAA ARL

644 READY Website (<http://www.arl.noaa.gov/HYSPLIT.php>), NOAA Air  
645 Resources Laboratory, Silver Spring, MD, 2014.

646 Du, H. H., Kong, L. D., Cheng, T. T., Chen, J. M., Du, J. F., Li, L., Xia,  
647 X., Leng, C. P., and Huang, G. H.: Insights into summertime haze  
648 pollution events over Shanghai based on online water-soluble ionic  
649 composition of aerosols, *Atmos. Environ.*, 45, 5131-5137, 2011.

650 Du, J. F., Cheng, T. T., Zhang, M., Chen, J. M., He, Q. S., Wang, X. M.,  
651 Zhang, R. J., Tao, J., Huang, G. H., Li, X., and Zha, S. P.: Aerosol size  
652 spectra and particle formation events at urban Shanghai in eastern China,  
653 *Aerosol and Air Quality Research*, 12, 1362-1372, 2012.

654 Dumka, U. C., Krishna Moorthy, K., Kumar, R., Hegde, P., Sagar, R.,  
655 Pant, P., Singh, N., and Suresh Babu, S.: Characteristics of aerosol black  
656 carbon mass concentration over a high altitude location in the Central  
657 Himalayas from multi-year measurements, *Atmos. Res.*, 96, 510-521,  
658 2010.

659 Ehn, M., Thornton, J. A., Kleist, E., Sipilä, M., Junninen, H., Pullinen, L.,  
660 Springer, M., Rubach, F., Tillmann, R., Lee, B., Lopez-Hilfiker, F.,  
661 Andres, S., Acir, I. H., Rissanen, M., Jokinen, T., Schobesberger, S.,  
662 Kangasluoma, J., Kontkanen, J., Nieminen, T., Kurtén, T., Nielsen, L. B.,  
663 Jørgensen, S., Kjaergaard, H. G., Canagaratna, M., Maso, M. D., Berndt,  
664 T., Petäjä, T., Wahner, A., Kerminen, V. -M., Kulmala, M., Worsnop, D.  
665 R., Wildt, J., and Mentel., T. F.: A large source of low-volatility

666 secondary organic aerosol, *Nature*, 506, 476-479, 2014.

667 Fuchs, N. A. and Sutugin, A. G.: High-dispersed aerosols in *Topics in*  
668 *Current Aerosol Research*, edited by: Hidy, G. M. and Brock, J. R.,  
669 Pergamon, Oxford, 2, 1-60, 1971.

670 Gao, J., Chai, F. H., Wang, T., Wang, S. L., and Wang, W. X.: Particle  
671 number size distribution and new particle formation: New characteristics  
672 during the special pollution control period in Beijing, *J. Environ. Sci.*,  
673 24, 14-21, 2012.

674 Gaydos, T. M., Stanier, C. O., and Pandis, S. N.: Modeling of in situ  
675 ultrafine atmospheric particle formation in the eastern United States, *J.*  
676 *Geophys. Res.*, 110 (D7), doi: 10.1029/2004JD004683, 2005.

677 Ghan, S. J., Easter, R. C., Chapman, E. G., Abdul-Razzak, H., Zhang, Y.,  
678 Leung, L. R., Laulainen, N. S., Saylor, R. D., and Zaveri, R. A.: A  
679 physically based estimate of radiative forcing by anthropogenic sulfate  
680 aerosol, *J. Geophys. Res.*, 106, 5279-5293, 2001.

681 Gong, Y. G., Hu, M., Cheng, Y. F., Su, H., Yue, D. L., Liu, F.,  
682 Wiedensohler, A., Wang, Z. B., Kalesse, H., Liu, S., Wu, Z. J., Xiao, K.  
683 T., Mi, P. C., and Zhang, Y. H.: Competition of coagulation sink and  
684 source rate: New particle formation in the Pearl River Delta of China,  
685 *Atmos. Environ.*, 44, 3278-3285, 2010.

686 Hansen, A. D. A., H. Rosen, and T. Novakov.: The aethalometer-an  
687 instrument for the real-time measurement of optical absorption by

688 aerosol particles, *Sci. Total Environ.*, 36, 191-196, 1984.

689 Hennigan, C. J., Westervelt, D. M., Riipinen, I., Engelhart, G. J., Lee, T.,  
690 Collett, J. L., Pandis, S. N., Adams, P. J., and Robinson, A. L.: New  
691 particle formation and growth in biomass burning plumes: An important  
692 source of cloud condensation nuclei, *Geophys. Res. Lett.*, 39, L09805,  
693 doi: 10.1029/2012GL050930, 2012.

694 Hildebrandt, R. L., Smith, J., Riipinen, I., Barsanti, K., Fry, J., Yli-Juuti,  
695 T., Petaja, T., Kulmala, M., and McMurry, P. H.: The role of nitrate in  
696 the formation of atmospheric nanoparticles: insights from ambient  
697 measurements and chemical transport models, (611f) Environmental  
698 division, American Institute of Chemical Engineers Annual Meeting,  
699 Pittsburgh, PA, 1 November 2012, 2012.

700 Huang, Y. L., Li, L., Li, J. Y., Wang, X., Chen, H., Chen, J. M., Yang, X.,  
701 Cross, D. S., Wang, H., Qiao, L. P., and Chen, H.: A case study of the  
702 highly time-resolved evolution of aerosol chemical and optical  
703 properties in urban Shanghai, China, *Atmos. Chem. Phys.*, 13,  
704 3931-3944, doi:10.5194/acp-13-3931-2013, 2013.

705 Hudson, J. G., and Noble, S.: CCN and vertical velocity influences on  
706 droplet concentrations and supersaturations in clean and polluted stratus  
707 clouds, *J. Atmos. Sci.*, 106, 24119-24126, 2014.

708 Hussein, T., Martikainen, J., Junninen, H., Sogacheva, L., Wagner, R.,  
709 Dal Maso, M., Riipinen, I., Aalto, P. P., and Kulmala, M.: Observation



710 of regional new particle formation in the urban atmosphere, *Tellus B*, 60,  
711 609-521, doi:10.1111/j.1600-0889.2008.00365.x, 2008.

712 IPCC: Climate Change 2013: The Physical Science Basis. Contribution of  
713 Working Group I to the Fifth Assessment Report of the  
714 Intergovernmental Panel on Climate Change, edited by: Jousaume, S.,  
715 Penner, J., and Tangang, F., IPCC, Stockholm, 2013.

716 Kerminen, V. -M.: How significantly does coagulation scavenging limit  
717 atmospheric particle production?, *J. Geophys. Res.*, 106, 24119-24126,  
718 2001.

719 Kerminen, V. -M., Lihabainen, H., Lomppula, M., Viisanen, Y., and  
720 Kulmala, M.: Direct observational evidence linking atmospheric aerosol  
721 formation and cloud droplet activation, *Geophys. Res. Lett.*, 32, L14803,  
722 doi: 10.1029/2005GL023130, 2005.

723 Kerminen, V. -M., Paramonov, M., Anttila, T., Riipinen, I., Fountoukis, C.,  
724 Korhonen, C., Asmi, E., Laakso, L., Lihavainen, H., Swietlicki, E.,  
725 Svenningsson, B., Asmi, A., Pandis, S. N., Kulmala, M., and Petäjä, T.:  
726 Cloud condensation nuclei production associated with atmospheric  
727 nucleation: a synthesis based on existing literature and new results,  
728 *Atmos. Chem. Phys.*, 12, 12037-12059, doi:10.5194/acp-12-12037-2012,  
729 2012.

730 Köhler, H.: The nucleus in and the the growth of hygroscopic droplets, *T.*  
731 *Faraday Soc.*, 32, 1152-1161, 1936.

732 Kristensson, A., Dal Maso, M., Swietlicki, E., Hussein, T., Zhou, J.,  
733 Kerminen, V. -M, and Kulmala, M.:Characterization of new particle  
734 formation events at a background site in Southern Sweden: relation to  
735 air mass history, *Tellus* 60B, 330-344,  
736 doi:10.1111/j.1600-0889.2008.00345.x, 2008.

737 Kumala, M., Dal Maso, M., Mäkelä, J. M., Pirjola, L., Väkevä, M., Aalto,  
738 P., Miikkulainen, P., Hämeri, K., and O'Dowd, C. D.: On the formation,  
739 growth and composition of nucleation mode particles, *Tellus B*, 53,  
740 479-490, 2001.

741 Kulmala, M., Laakso, L., Lehtinen, K. E. J., Riipinen, I., Dal Maso, M.,  
742 Anttila, T., Kerminen, V. -M., Hörrak, U., Vana, M., and Tammet, H.:  
743 Initial steps of aerosol growth, *Atmos. Chem. Phys.*, 4, 2553-2560,  
744 doi:10.5194/acp-4-2553-2004, 2004.

745 Kulmala, M., Petäjä, T., Mönkkönen, P., Koponen, I. K., Dal Maso, M.,  
746 Aalto, P. P., Lehtinen, K. E. J., and Kerminen, V. -M.: On the growth of  
747 nucleation mode particles: source rates of condensable vapor in polluted  
748 and clean environments, *Atmos. Chem, Phys.*, 5, 409-416,  
749 doi:10.5194/acp-5-409-2005, 2005.

750 Kulmala, M., Kontkanen, J., Junninen, H., Lehtipalo, K., Manninen, H. E.,  
751 Nieminen, T., Petäjä, T., Sipilä, M., Schobesberger, S., Rantala, P.,  
752 Franchin, A., Jokinen, T., Järvinen, E., Äijälä, M., Kangasluoma, J.,  
753 Hakala, J., Aalto, P. P., Paasonen, P., Mikkilä, J., Vanhanen, J., Aalto, J.,

754 Hakola, H., Aakkonen, U., Ruuskanen, T., Mauldin III, R. L., Duplissy,  
755 J., Vehkamäki, H., Bäck, J., Kortelainen, A., Riipinen, L., Kurtén, T.,  
756 Johnston, M. V., Smith, J. N., Ehn, M., Mentel, T. F., Lehtinen, K. E. J.,  
757 Laaksonen, A., Kerminen, V. -M., and Worsnop, D. R.: Direct  
758 observations of atmospheric aerosol nucleation, *Science*, 339, 943-946,  
759 2013.

760 Kulmala, M., Petäjä T., Nieminen, T., Sipilä M., Manninen, H. E.,  
761 Lehtipato, K., Dal Maso, M., Aalto, P. P., Junninen, H., Paasonen, P.,  
762 Riipinen, I., Lehtinen, K. E., Laaksonen, A., and Kerminen, V. -M.:  
763 Measurement of the nucleation of atmospheric aerosol particles, *Nat.*  
764 *Protoc.*, 7, 1651–1667, 2012.

765 Kuwata, M. and Kondo, Y.: Dependence of size-resolved CCN spectra on  
766 the mixing state of nonvolatile cores observed in Tokyo. *J. Geophys.*  
767 *Res.*, 113, D19202, doi; 10.1029/2007JD009761, 2008.

768 Laakso, L., Merikanto, J., Vakkari, V., Laakso, H., Kulmala, M., Molefe,  
769 M., Kgabi, N., Mabaso, D., Carslaw, K. S., Spracklen, D. V., Lee, L. A.,  
770 Reddington, C. L., and Kerminen, V. -M.: Boundary layer nucleation as  
771 a source of new CCN in savannah environment, *Atmos. Chem. Phys*, 13,  
772 1957-1972, doi:10.5194/acp-13-1957-2013, 2013.

773 Laaksonen, A., Hamed, A., Joutsensaari, J., Hiltunen, L., Cavalli, F.,  
774 Junkermann, W., Asmi, A., Fuzzi, S., and Facchini, M. C.: Cloud  
775 condensation nucleus production from nucleation events at a highly

776 polluted region, *Geophys. Res. Lett.*, 32, L06812, doi;  
777 10.1029/2004GL022092, 2005.

778 Lance, S., Medina, J., Smith, J. N., and Nenes, A.: Mapping the operation  
779 of the DMT Continuous Flow CCN counter, *Aerosol Sci. Tech.*, 40,  
780 242-254, 2006.

781 Leng, C. P., Cheng, T. T., Chen, J. M., Zhang, R. J., Tao, J., Huang, G. H.,  
782 Zha, S. P., Zhang, M. G., Fang, W., Li, X., and Li, L.: Measurements of  
783 surface cloud condensation nuclei and aerosol activity in downtown  
784 Shanghai, *Atmos. Environ.*, 69, 354-361, 2013.

785 Lihavainen, H., Kerminen, V. -M., Komppula, M., Hatakka, J., Aaltonen,  
786 V., Kulmala, M., and Viisanen, Y.: Production of “potential” cloud  
787 condensation nuclei associated with atmospheric new particle formation  
788 in north Finland, *J. Geophys. Res.*, 108, D24, 4872, doi;  
789 10.1029/2003JD003887, 2003.

790 Lohmann, U. and Feichter, J.: Global indirect aerosol effect; a review,  
791 *Atmos. Chem. Phys.*, 5, 715-737, doi:10.5194/acp-5-715-2005, 2005.

792 McMurry, P. H., Takano, H., and Anderson, G. R.: Study of the ammonia  
793 (gas)-sulphuric acid (aerosol) reaction rate, *Enviro. Sci. and Tech*, 17,  
794 347-352, 1983.

795 McMurry, P. H., Fink, M., Sakurai, H., Stolzenburg, M. R., Mauldin, R.  
796 L., Smith, J., Eisele, F., Moore, K., Sjostedt, S., Tanner, D., Huey, L. G.,  
797 Nowak, J. B., Edgerton, E., and Voisin, D.: A criterion for new particle

798 formation in the sulfur-rich Atlanta atmosphere, *J. Geophys. Res.*, 110,  
799 D22S02, doi; 10.1029/2005JD005907, 2005.

800 Merikanto, J., Sprackken, D. V., Mann, G. W., Pickering, S. J and Carslaw,  
801 K. S.: Impact of nucleation on global CCN, *Atmos. Chem. Phys.*, 9(21),  
802 8601-8616, doi:10.5194/acp-9-8601-2009, 2009.

803 Metzger, A., Verheggen, B., Dommen, J., Duplissy, J., Prevot, A. S.,  
804 Weingartner, E., Riipinen, I., Kulmala, M., Spracklen, D. V., Carslaw, K.  
805 S., and Baltensperger, U.: Evidence for the role of organic in aerosol  
806 particle formation under atmospheric conditions, *P. Natl. Acad. Sci.*  
807 USA, 107, 6646-6651, 2010.

808 Mönkkönen, P., Koponen, I. K., Lehtinen, K. E. J., Hämeri, K., Uma, R.,  
809 and Kulmala, M.: Measurement in a highly polluted Asian mega city:  
810 observations of aerosol number size distribution, modal parameters and  
811 nucleation events, *Atmos. Chem. Phys.*, 5, 57-66,  
812 doi:10.5194/acp-5-57-2005, 2005.

813 Nieminen, T., Manninen, H. E., Sihto, S. L., Yli-Juuti, T., Mauldin, R. L.,  
814 Petaja, T., Riipinen, I., Kerminen, V. -M., and Kulmala, M.: Connection  
815 of sulfuric acid to atmospheric nucleation in boreal forest, *Environ. Sci.*  
816 *Technol.*, 43, 4715-4721, 2009.

817 O'Dowd, C. D.: Biogenic coastal aerosol production and its influence on  
818 aerosol radiative properties, *J. Geophys Res.*, 106, 1545-1549, 2001.

819 O'Dowd, C. D., Aalto, P., Hameri, K., Kulmala, M., and Hoffmann, T.:

820 Atmospheric particles from organic vapors, *Nature*, 416, 497-498, 2002.

821 Paasonen, P., Nieminen, T., Asmi, E., Manninen, H. E., Petäjä, T.,  
822 Plass-Dülmer, C., Flentje, H., Birmili, W., Wiedensahler, A., Hörrak, U.,  
823 Metzger, A., Hamed, A., Laaksonen, A., Facchini, M. C., Kerminen, V.  
824 M., and Kulmala, M.: On the role of sulphuric acid and low-volatility  
825 organic vapors in the initial steps of atmospheric new particle formation,  
826 *Atmos. Chem. Phys.*, 10, 11223-11242, doi:10.5194/acp-10-11223-2010,  
827 2010.

828 Petäjä, T., Mauldin, R. L., Kosciuch, E., McGrath, J., Nieminen, T.,  
829 Paasonen, P., Boy, M., Adamov, A., Kotiaho, T., and Kulmala, M.:  
830 Sulfuric acid and OH concentrations in a boreal forest site, *Atmos.*  
831 *Chem. Phys.*, 9, 7435-7448, doi: 10.5194/acp-9-7435-2009, 2009.

832 Petters, M. D., and Kreidenweis, S. M.: A single parameter representation  
833 of hygroscopic growth and cloud condensation nucleus activity, *Atmos.*  
834 *Chem. Phys.*, 7, 1961-1971, doi:10.5194/acp-7-1961-2007, 2007.

835 Petzold, A., Kopp, C., and Niessner, R.: The dependence of the specific  
836 attenuation cross-section on black carbon mass fraction and particle size,  
837 *Atmos. Environ.*, 31, 661-672, 1997.

838 Pierce, J. R., and Adams, P. J.: Efficiency of cloud condensation nuclei  
839 formation from ultrafine particles, *Atmos. Chem. Phys.*, 7, 1367-1379,  
840 doi:10.5194/acp-7-1367-2007, 2007.

841 Pierce, J. R., and Adams, P. J.: Uncertainty in global CCN concentrations

842 from uncertain aerosol nucleation and primary emission rates, *Atmos.*  
843 *Chem. Phys.*, 9, 1339-1356, doi:10.5194/acp-9-1339-2009, 2009.

844 Ramanathan, V., Crutzen, P. J., Kiehl, J. T., and Rosenfeld, D.: Aerosols,  
845 Climate, and the Hydrological Cycle, *Science*, 294, 2119-2124, 2001.

846 Riipinen, I., Pierce, J. R., Yli-Juuti, T., Nieminen, T., Häkkinen, S., Ehn,  
847 M., Junnunen, H., Lehtipalo, K., Petäjä, T., Slowik, J., Chang, R.,  
848 Shantz, N. C., Abbatt, J., Leaitch, W. R., Kerminen, V. -M., Worsnop, D.  
849 R., Pandis, S. N., Donahue, N. M., and Kulmala, M.: Organic  
850 condensation: a vital link connecting aerosol formation to cloud  
851 condensation nuclei (CCN) concentrations, *Atmos. Chem. Phys.*, 11,  
852 3865-3878, doi:10.5194/acp-11-3865-2011, 2011.

853 Roberts, G. C. and Nenes, A.: A continuous-flow streamwise  
854 thermal-gradient CCN chamber for atmospheric measurements, *Aerosol*  
855 *Sci. Tech.*, 39, 206-221, 2006.

856 Sakurai, T., Fujita, S. I., Hayami, H., and Furuhashi, N.: A study of  
857 atmospheric ammonia by means of modeling analysis in the Kanto  
858 region of Japan, *Atmos. Environ.*, 39, 203-210, 2005.

859 Shen, X. J., Sun, J. Y., Zhang, Y. M., Wehner, B., Nowak, A., Tuch, T.,  
860 Zhang, X. C., Wang, T. T., Zhou, H. G., Zhang, X. L., Dong, F., Birmili,  
861 W., and Wiedensohler, A.: First long-term study of particle number size  
862 distributions and new particle formation events of regional aerosol in the  
863 North China Plain, *Atmos. Chem. Phys.*, 11, 1565-1580,

864 doi:10.5194/acp-11-1565-2011, 2011.

865 Smith, J. N., Moore, K. F., McMurry, P. H., and Eisele F. L.: Atmospheric  
866 measurements of sub-20 nm diameter particle chemical composition by  
867 thermal desorption chemical ionization mass spectrometry, *Aerosol Sci.*  
868 *Technol*, 38, 100-110, 2004.

869 Spracklen, D. V., Carslaw, K. S., Kulmala, M., Kerminen, V. M., Mann, G.  
870 W., and Sihto, S. L.: The contribution of boundary layer nucleation  
871 events to total particle concentrations on regional and global scales,  
872 *Atmos. Chem. Phys.*, 6, 5631-5648, doi:10.5194-acp-6-5631-2006,  
873 2006.

874 Spracklen, D. V., Carslaw, K. S., Kulmala, M., Kerminen, V. M., Sihto, S.  
875 L., Riipinen, I., Merikanto, J., Mann, g. w., Chipperfield, M. P.,  
876 Wiedensohler, A., Birmili, W., and Lihavainen, H.: Contribution of  
877 particle formation to global cloud condensation nuclei concentrations,  
878 *Geophys. Res. Lett.*, 35, L06808, doi:10.1029/2007GL033038, 2008.

879 Vehkamäki, H., Dal Maso, M., Hussein, T., Flannagan, R., Hyvärinen, A.,  
880 Lauros, J., Merikanto, J., Mönkkönen, P., Pihlatie, M., Salminen, K.,  
881 Sogacheva, L., Thum, T., Ruuskanen, T. M., Keronen, P., Aalto, P. P.,  
882 Hari, P., Lehtinen, K. E. J., Rannik, Ü., and Kulmala, M.: Atmospheric  
883 particle formation events at Värriö measurement station in Finnish  
884 Lapland 1998-2002, *Atmos. Chem. Phys.*, 4, 2015-2023,  
885 doi:10.5194/acp-4-2015-2004, 2004.



886 Vuollekoski, H., Kerminen, V. -M., Anttila, T., Sihto, S. L., Vana, M., Ehn,  
887 M., Korhonen, H., McFiggans, G., O'Dowd, C. D., and Kulmala, M.:  
888 Iodine dioxide nucleation simulations in coastal and remote marine  
889 environments, *J. Geophys. Res.*, 114, D00206, doi:  
890 10.1029/2008JD010713, 2009.

891 Wang, X. F., Zhang, Y. P., Chen, H., Yang, X., and Chen, J. M.: Particle  
892 nitrate formation in a highly polluted urban area: a case study by  
893 single-particle mass spectrometry in Shanghai, *Environ. Sci. Technol.*,  
894 43, 3061-3066, 2009.

895 Wang, Y., Zhuang, G. S., Zhang, X. Y., Huang, K., Xu, C., Tang, A. H.,  
896 Chen, J. M., and An, Z. S.: The ion chemistry, seasonal cycle, and  
897 sources of PM<sub>2.5</sub> TSP aerosol in Shanghai, *Atmos. Environ.*, 40,  
898 2935-2952, 2006.

899 Wang, Z. B., Hu, M., Sun, J. Y., Wu, Z. J., Yue, D. L., Shen, X. J., Zhang,  
900 Y. M., Pei, X. Y., Cheng, Y. F., and Wiedensohler, A.: Characteristics of  
901 regional new particle formation in urban and regional background  
902 environments in the North China Plain, *Atmos. Chem. Phys.*, 13,  
903 12495-12506, 3013.

904 Wang, Z. B., Hu, M., Wu, Z. J., and Yue, D. L., Research on the  
905 formation mechanism of new particles in the atmosphere, *Acta Chim.*  
906 *Sinica*, 71, 519-527, 2013.

907 Weber, R. J., Marti, J. J., McMurry, P. H., Eisele, F. L., Tanner, D. J., and

908 Jefferson, A.: Measured atmospheric new particle formation rates:  
909 Implications for nucleation mechanisms, *Chem. Eng. Commun.*, 151,  
910 53-64, 1996.

911 Weber, R. J., McMurry, P. H., Mauldin, R. L., Tanner, D. J., Eisele, F. L.,  
912 Clarke, A. D., and Kapustin, V. N.: New particle formation in the remote  
913 troposphere: a comparison of observations at various sites, *Geophys.*  
914 *Res. Lett.*, 26, 307-310, doi:10.1029/1998GL900308, 1999.

915 Weingartner, E., Saathoff, H., Schnaiter, M., Streit, N., Bitnar, B., and  
916 Baltensperger, U.: Absorption of light by soot particles: determination of  
917 the absorption coefficient by means of aethalometers, *J. Aerosol Sci.*, 34,  
918 1445-1463, 2003.

919 Wiedensohler, A., Cheng, Y. F., Nowak, A., Wehner, B., Achtert, P.,  
920 Berghof, M., Birmili, W., Wu, Z. J., Hu, M., Zhu, T., Takegawa, N., Kita,  
921 K., Kondo, Y., Lou, S. R., Hofzumahaus, A., Holland, F., Wahner, A.,  
922 Gunthe, S. S., Rose, D., Su, H., and Pöschl, U.: Rapid aerosol growth  
923 and increase of cloud condensation nucleus activity by secondary  
924 aerosol formation and condensation: a case study for regional air  
925 pollution in northeastern China, *Geophys. Res. Lett.*, 114, D00G08,  
926 doi:10.1029/2008JD010884, 2009

927 Wu, Z., Hu, M., Liu, S., Wehner, B., Bauer, S., Määbling, A., Wiedensohler,  
928 A., Petäjä, T., Dal Maso, M., and Kulmala, M.: New particle formation  
929 in Beijing, China: statistical analysis of a 1-year dataset, *J. Geophys.*

930 Res., 112, D09209, doi; 10.1029/2006JD007406, 2007.

931 Wu, Z. J., Hu, M., Lin, P., Liu, S., Wehner, B., and Wiedensohler, A.:  
932 Particle number size distribution in the urban atmosphere of Beijing,  
933 China, Atmos. Environ., 42, 7967-7980,  
934 doi:10.1016/j.atmosenv.2008.06.022, 2008.

935 Yu, F. Q.: Effect of ammonia on new particle formation: a kinetic  
936  $\text{H}_2\text{SO}_4\text{-H}_2\text{O-NH}_3$  nucleation model constrained by laboratory  
937 measurements, J. Geophys. Res., 111, D01204, doi;  
938 10.1029/2005JD005968, 2006.

939 Yu, F., Wang, Z., Luo, G., and Turco, R.: Ion-mediated nucleation as an  
940 important global source of tropospheric aerosols, Atmos. Chem. Phys., 8,  
941 2537-2554, doi:10.5194/acp-8-2537-2008, 2008.

942 Yu, H., McGraw, R., and Lee, S. H.: Effects of amines on formation of  
943 sub-3 nm particles and their subsequent growth, Geophys. Res. Lett., 39,  
944 L02807, doi: 10.1029/2011GL050099, 2012.

945 Yue, D. L., Hu, M., Zhang, R. J., Wu, Z. J., Su, H., Wang, Z. B., Peng, J.  
946 F., He, L. Y., Huang, X. F., Gong, Y. G., and Wiedensohler, A.: Potential  
947 contribution of new particle formation to cloud condensation nuclei in  
948 Beijing, Atmos. Environ., 45, 6070-6077, 2011.

949 Zhang, R. J., Jing, J. S., Tao, J., Hsu, S.-C., Wang, G., Cao, J. J., Lee, C. S.  
950 L., Zhu, L., Chen, Z., Zhao, Y., and Shen, Z.: Chemical characterization  
951 and source apportionment of  $\text{PM}_{2.5}$  in Beijing: seasonal perspective,

952 Atmos. Chem. Phys., 13, 7053-7074, doi:10.5194/acp-13-7053-2013,  
953 2013.

954 Zhang, R. Y.: Getting to the critical nucleus of aerosol formation, Science,  
955 328, 1366-1367, 2010.

956 Zhang, R. Y., Khalizov, A., Wang, L., Hu, M., and Xu, W.: Nucleation  
957 and growth of nanoparticles in the atmosphere, Chem. Rev., 112,  
958 1957-2011, 2012.

959 Zheng, J., Hu, M., Zhang, R., Yue, D., Wang, Z., Guo, S., Li, X., Bohn, B.,  
960 Shao, M., He, L., Huang, X., Wiedensohler, A., and Zhu, T.:  
961 Measurements of gaseous H<sub>2</sub>SO<sub>4</sub> by AP-ID-CIMS during CAREBijng  
962 2008 Campaign, Atmos. Chem. Phys., 11, 7755-7765,  
963 doi:10.5194/acp-11-7755-2011, 2011.

964

965

966

967

968

969

970

971

972

973

974 **Table 1.** Comparison of CCN enhancement ratios from NPF events with  
 975 different formation and growth rates.

	0.2%	0.4%	0.6%	0.8%	1.0%
Enhancement ratio (FR>0.40)	1.18	1.84	1.88	1.84	1.77
Enhancement ratio (FR<0.40)	1.15	1.89	1.81	1.77	1.58
Enhancement ratio (GR>4.91)	1.25	1.95	2.03	1.93	1.72
Enhancement ratio (GR<4.91)	1.10	1.79	1.80	1.74	1.63

976

977 **Table 2.** Effective hygroscopicity parameters ( $\kappa$ ) and densities of the four  
 978 category compositions.

Species	Data source	$\kappa$	Density (g cm <sup>-3</sup> )
Sulfate & nitrate	SO <sub>4</sub> <sup>2-</sup> +NO <sub>3</sub> <sup>-</sup> +NH <sub>4</sub> <sup>+</sup>	0.6	1.7
Sodium chloride	Cl <sup>-</sup> +Na <sup>+</sup>	1	2.2
Insoluble compounds	Others	0	2.0

979

980 **Figure captions**

981 **Figure 1.** Series of 10-min mean meteorological parameters over the  
 982 entire campaign.

983 **Figure 2.** Series of 5-min mean SO<sub>2</sub> and PM<sub>2.5</sub> concentration and  
 984 atmospheric visibility over the entire campaign.

985 **Figure 3.** Series of aerosol size distribution, 4-min mean total (N<sub>total</sub>) and  
 986 nucleation (N<sub>10-20nm</sub>) mode aerosol number concentration and 1-hour  
 987 mean CCN concentration over the entire campaign.

988 **Figure 4.** Temporal evolution of 4-min mean aerosol size spectra,  
989 showing new particle formation and subsequent growth on 3 and 4 April  
990 2012.

991 **Figure 5.** Temporal evolution of 10-min mean meteorological parameters  
992 during the new particle formation event on 3-4 April 2012.

993 **Figure 6.** Temporal evolutions of 5-min mean atmospheric visibility, BC  
994 and  $PM_{2.5}$  concentrations during the new particle formation event on 3-4  
995 April 2012.

996 **Figure 7.** Temporal evolutions of 4-min mean mode, median and  
997 diameters and 10-20 nm particle concentration, showing the growth rate  
998 and formation of new particle on 3-4 April 20.

999 **Figure 8.** Series of 1-h mean  $SO_2$ ,  $SO_4^{2-}$ ,  $NO_3^-$  and  $NH_4^+$  concentrations  
1000 on 3 and 4 April 2012.

1001 **Figure 9.** Series of 1-h mean CCN concentration and CCN/CN on 3 and  
1002 4 April 2012.

1003 **Figure 10.** Scatterplots of predicted and measured CCN concentrations at  
1004 different *SS* conditions, the red dash line represents  $y=x$ .

1005

1006

1007

1008

1009

1010

1011

1012

1013

1014

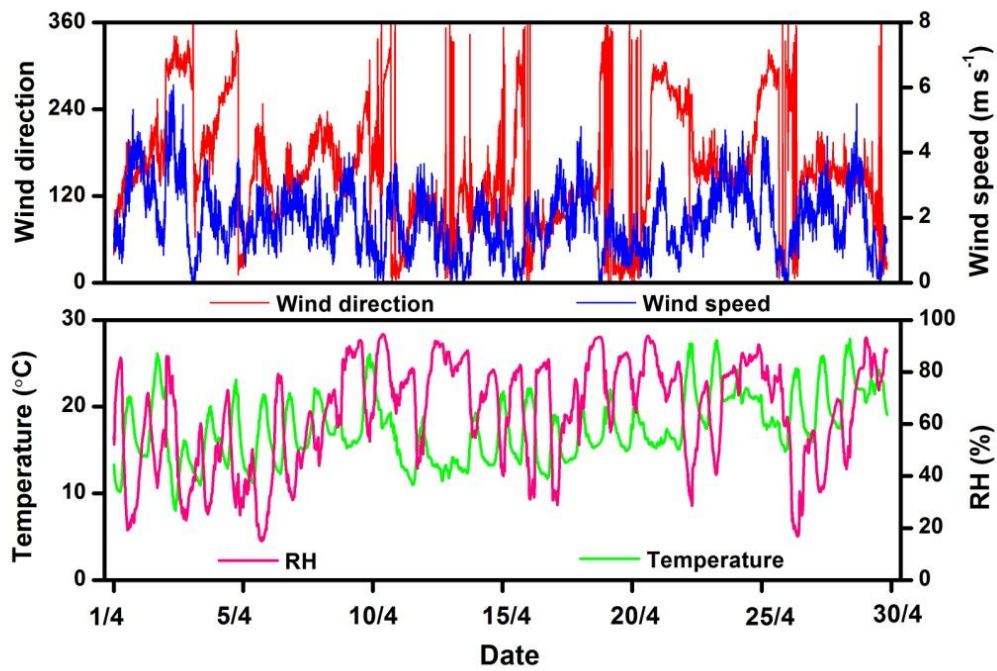
1015

1016

1017

1018

1019



1020 Figure 1. Series of 10-min mean meteorological parameters over the  
1021 entire campaign.

1022

1023

1024

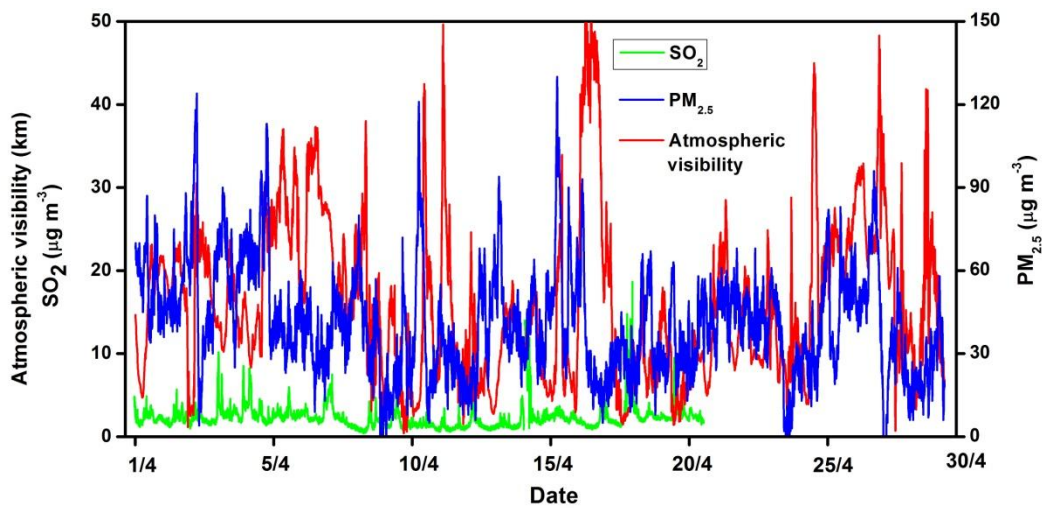
1025

1026

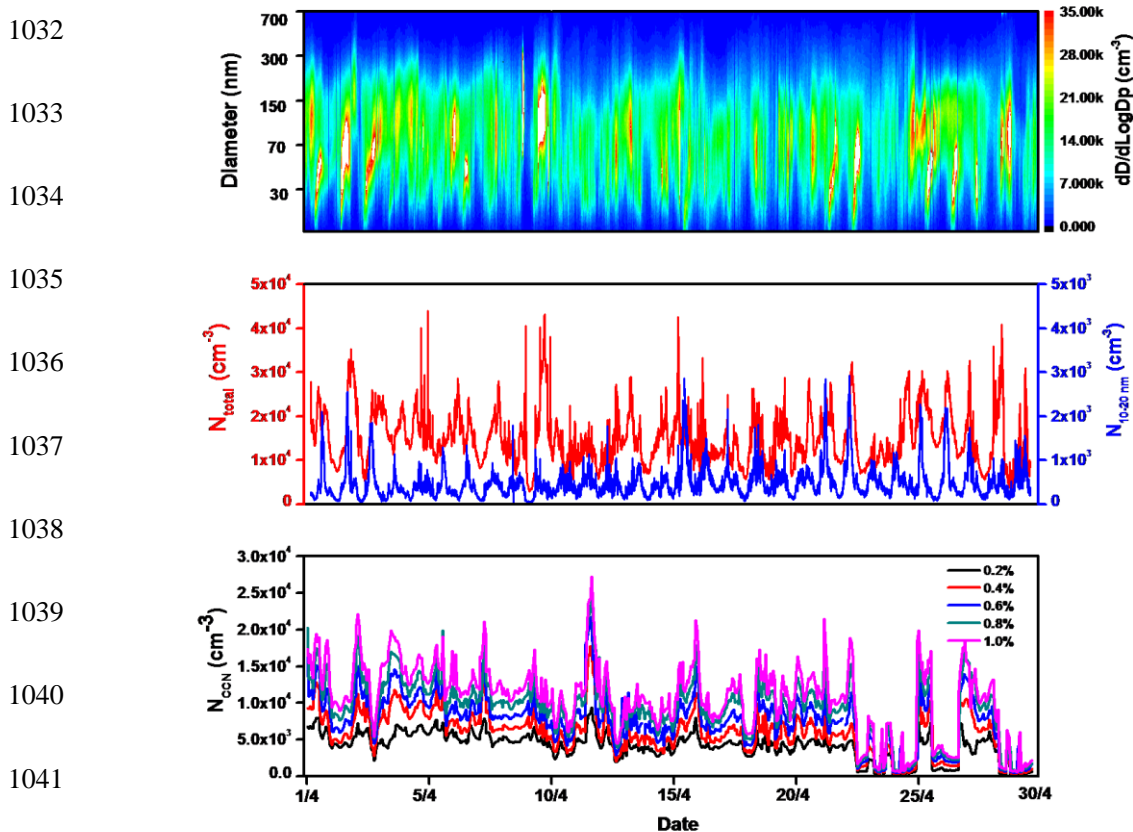
1027

1028

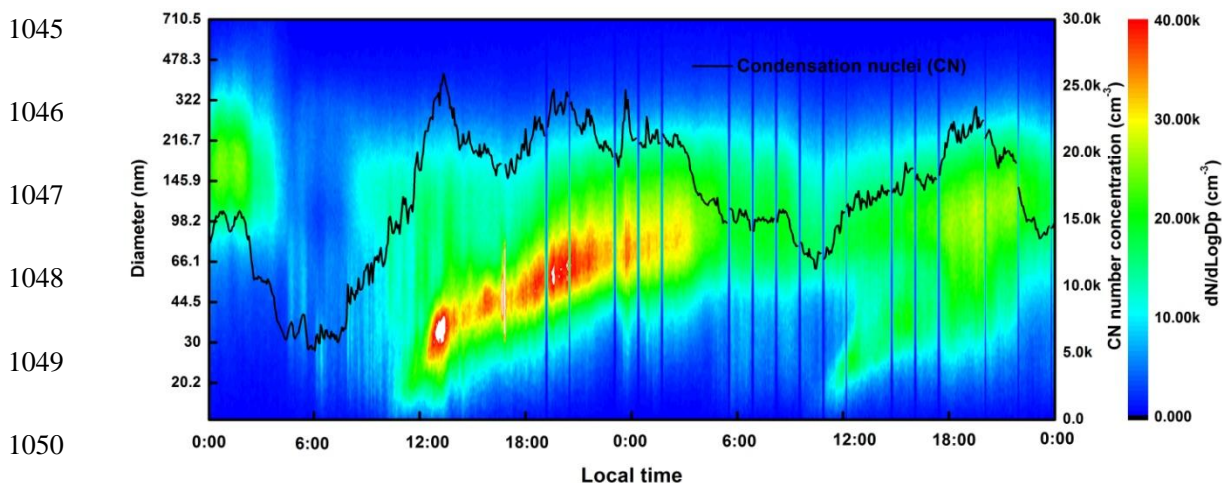
1029



1030 Figure 2. Series of 5-min mean  $\text{SO}_2$  and  $\text{PM}_{2.5}$  concentration and  
1031 atmospheric visibility over the entire campaign.



1032  
1033  
1034  
1035  
1036  
1037  
1038  
1039  
1040  
1041  
1042 Figure 3. Series of aerosol size distribution, 4-min mean total ( $N_{\text{total}}$ ) and  
1043 nucleation ( $N_{10-20\text{nm}}$ ) mode aerosol number concentration and 1-hour  
1044 mean CCN concentration over the entire campaign.



1045  
1046  
1047  
1048  
1049  
1050  
1051 Figure 4. Temporal evolution of 4-min mean aerosol size spectra,  
1052 showing new particle formation and subsequent growth on 3 and 4 April  
1053 2012.



1054

1055

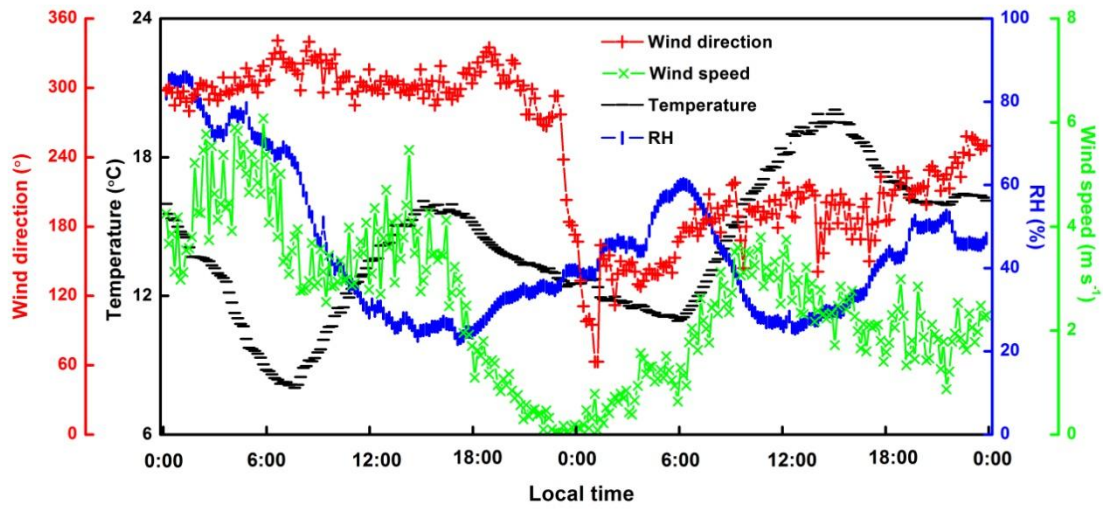
1056

1057

1058

1059

1060



1061

Figure 5. Temporal evolution of 10-min mean meteorological parameters

1062

during the new particle formation event on 3-4 April 2012.

1063

1064

1065

1066

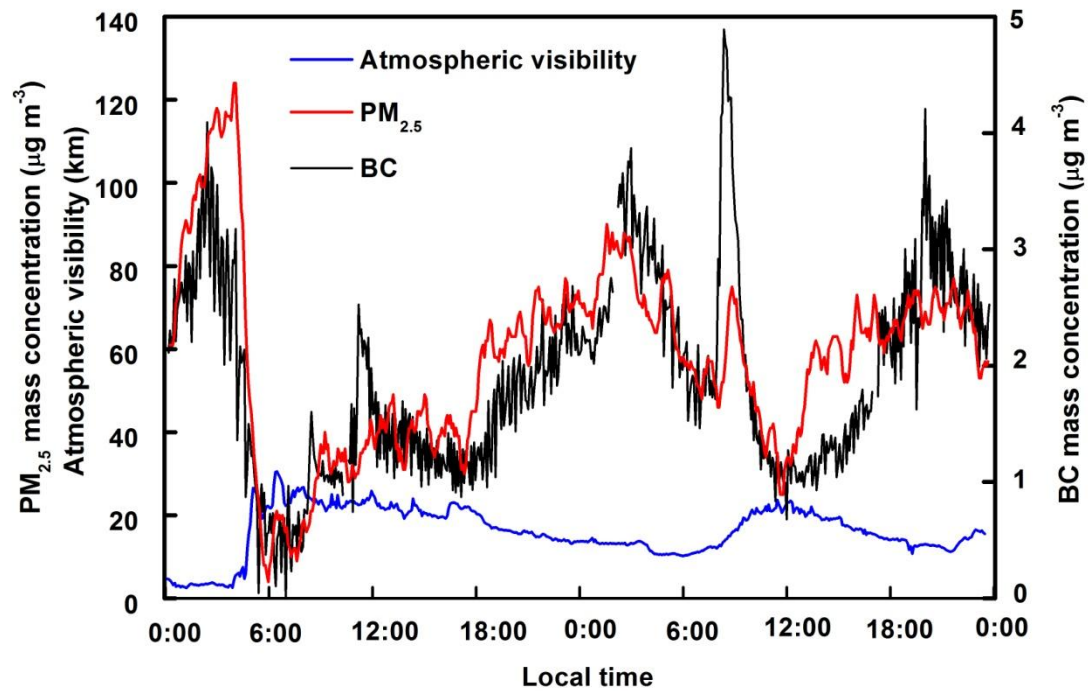
1067

1068

1069

1070

1071



1072

Figure 6. Temporal evolutions of 5-min mean atmospheric visibility, BC

1073

and  $PM_{2.5}$  concentrations during the new particle formation event on 3-4

1074

April 2012.

1075

1076

1077

1078

1079

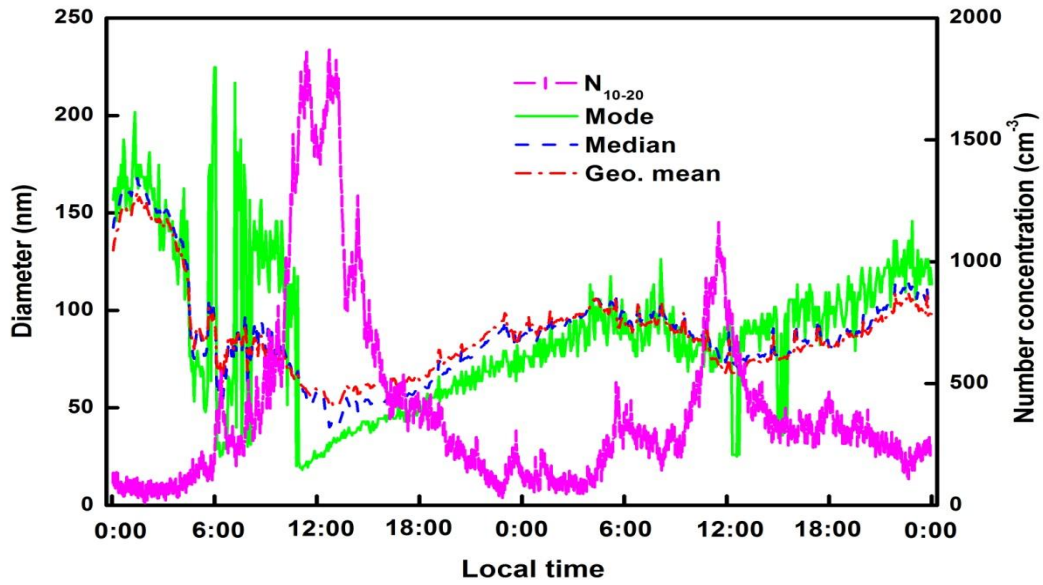
1080

1081

1082

1083

1084



1085 Figure 7. Temporal evolutions of 4-min mean mode, median and  
1086 diameters and 10-20 nm particle concentration, showing the growth rate  
1087 and formation of new particle on 3-4 April 20.

1088

1089

1090

1091

1092

1093

1094

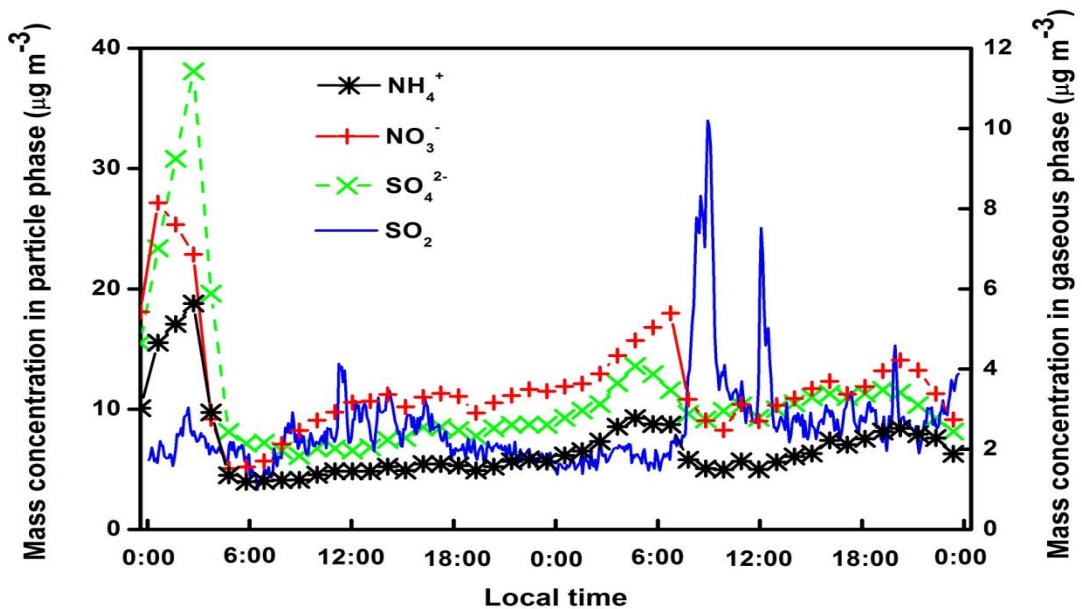
1095

1096

1097

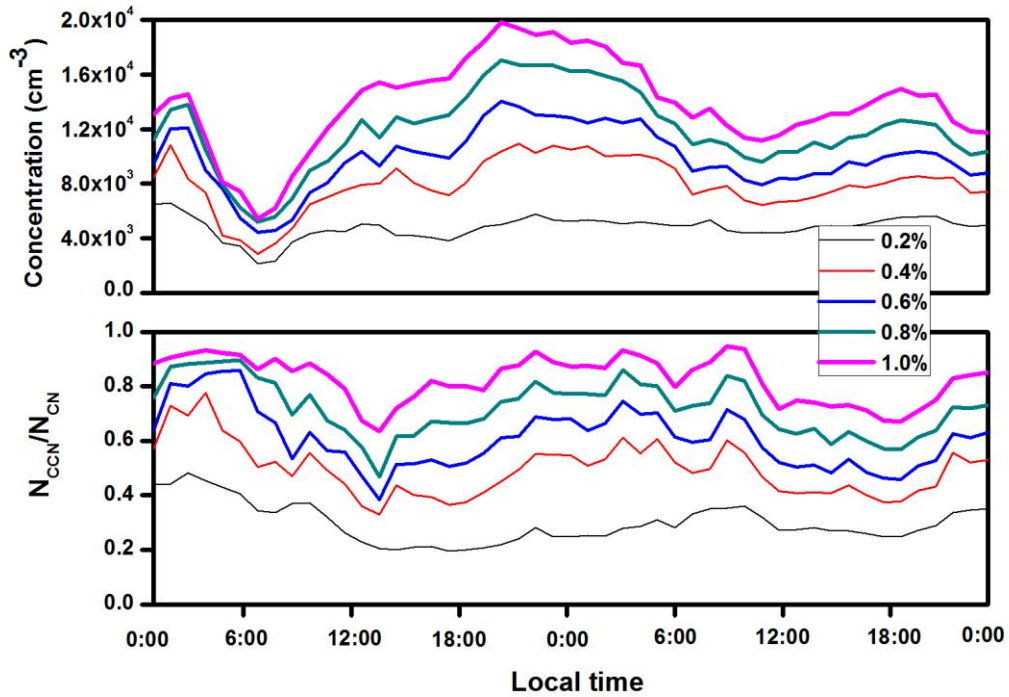
1098

1099



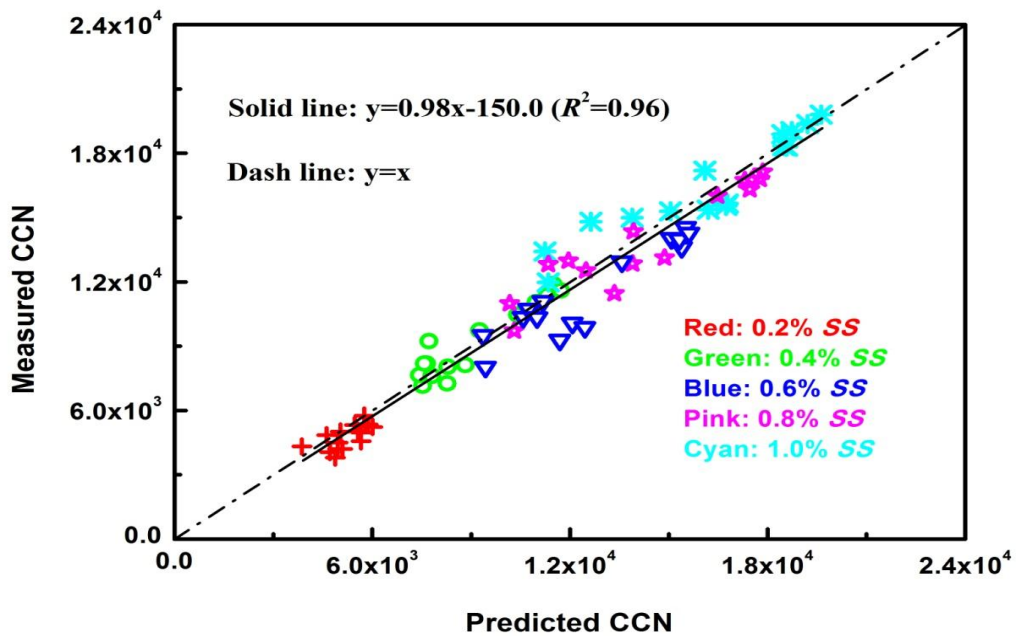
1101 Figure 8. Series of 1-h mean  $SO_2$ ,  $SO_4^{2-}$ ,  $NO_3^-$  and  $NH_4^+$  concentrations  
1102 on 3 and 4 April 2012.

1103  
1104  
1105  
1106  
1107  
1108  
1109  
1110  
1111  
1112  
1113  
1114  
1115  
1116  
1117  
1118



1119 Figure 9. Series of 1-h mean CCN concentration and CCN/CN on 3 and 4  
1120 April 2012.

1121  
1122  
1123  
1124  
1125  
1126  
1127  
1128  
1129  
1130  
1131  
1132  
1133  
1134  
1135



1136 Figure 10. Scatterplots of predicted and measured CCN concentrations at  
1137 different SS conditions, the red dash line represents  $y=x$ .